

## Au<sub>22</sub>Ir<sub>3</sub>(PET)<sub>18</sub>: An Unusual Alloy Cluster through Intercluster Reaction

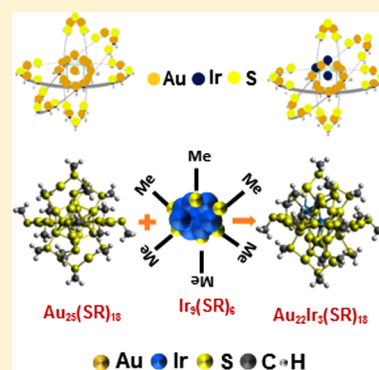
Shridevi Bhat,<sup>†,§</sup> Ananya Bakshi,<sup>†,§</sup> Sathish Kumar Mudedla,<sup>‡</sup> Ganapati Natarajan,<sup>†</sup> V. Subramanian,<sup>‡,Ⓛ</sup> and Thalappil Pradeep<sup>\*,†,Ⓛ</sup>

<sup>†</sup>DST Unit of Nanoscience (DST UNS) and Thematic Unit of Excellence, Department of Chemistry, Indian Institute of Technology Madras, Chennai 600036, India

<sup>‡</sup>Chemical Laboratory, CSIR-Central Leather Research Institute, Adyar, Chennai 600020, India

### **S** Supporting Information

**ABSTRACT:** An intercluster reaction between Au<sub>25</sub>(PET)<sub>18</sub> and Ir<sub>9</sub>(PET)<sub>6</sub> producing the alloy cluster, Au<sub>22</sub>Ir<sub>3</sub>(PET)<sub>18</sub> exclusively, is demonstrated where the ligand PET is 2-phenylethanethiol. Typical reactions of this kind between Au<sub>25</sub>(PET)<sub>18</sub> and Ag<sub>25</sub>(SR)<sub>18</sub>, and other clusters reported previously, produce mixed cluster products. The cluster composition was confirmed by detailed high-resolution electrospray ionization mass spectrometry (ESI MS) and other spectroscopic techniques. This is the first example of Ir metal incorporation in a monolayer-protected noble metal cluster. The formation of a single product was confirmed by thin layer chromatography (TLC). Density functional theory (DFT) calculations suggest that the most favorable geometry of the Au<sub>22</sub>Ir<sub>3</sub>(PET)<sub>18</sub> cluster is one wherein the three Ir atoms are arranged triangularly with one Ir atom at the icosahedral core and the other two on the icosahedral shell. Significant contraction of the metal core was observed due to strong Ir–Ir interactions.



Atomically precise noble metal nanoclusters are being intensely investigated currently in the context of their fundamental properties and potential applications.<sup>1</sup> Fundamental properties such as optical absorption over an extended window,<sup>2–5</sup> intense near-infrared luminescence,<sup>6–9</sup> biocompatibility,<sup>2,10,11</sup> varying chemical functionalities and associated properties,<sup>2,12,13</sup> and so forth are interesting features of these materials. Homogeneous catalysis in solution and heterogeneous catalysis in the supported form are some of the commonly investigated aspects of their science.<sup>2,14–16</sup> Despite various studies in the area, new developments in cluster catalysis demands new materials.<sup>14</sup> Creating nanoalloys by heteroatom incorporation into monolayer-protected clusters is a promising strategy to synthesize new materials with novel properties. Many such materials have been made by incorporating elements like Pd,<sup>17,18</sup> Ag,<sup>19</sup> Pt,<sup>20</sup> Cu,<sup>21,22</sup> Hg,<sup>23,24</sup> and so forth into magic cluster systems such as Au<sub>25</sub>(SR)<sub>18</sub>, and the properties of resulting alloys have been investigated thoroughly.

Recently, Krishnadas et al.<sup>25</sup> have demonstrated that intercluster reaction is a facile method for alloy cluster formation by taking Au<sub>25</sub>(SR)<sub>18</sub> and Ag<sub>44</sub>(SR)<sub>30</sub> as model systems. In yet another report,<sup>26</sup> they showed the structure and topology preserving conversion of monolayer-protected clusters upon reacting Au<sub>25</sub>(SR)<sub>18</sub> and Ag<sub>25</sub>(SR)<sub>18</sub>. Herein, we have used the reaction between Au<sub>25</sub>(PET)<sub>18</sub> and Ir<sub>9</sub>(PET)<sub>6</sub> as a method to create an unknown alloy cluster, Au<sub>22</sub>Ir<sub>3</sub>(PET)<sub>18</sub>. Unlike the previous cases,<sup>25,26</sup> these clusters react, forming a single alloy cluster.

The clusters Au<sub>25</sub>(PET)<sub>18</sub><sup>27–31</sup> and Ir<sub>9</sub>(PET)<sub>6</sub><sup>32</sup> were synthesized by reported methods and characterized by UV/vis absorption spectroscopy and mass spectrometry (Figures S1 and S2). These show well-defined mass spectral features at *m/z* 7393 and 2553, respectively. Electrospray ionization mass spectrometry (ESI MS) of Au<sub>25</sub>(PET)<sub>18</sub> is isotopically resolved and matches well with simulated spectrum. The simulated spectrum of Ir<sub>9</sub>(PET)<sub>6</sub> is fitted with the experimental spectrum; the latter, MALDI MS, is not isotopically resolved. The UV/vis absorption spectra show well-defined features as in the literature.<sup>3,32</sup> These clusters were used for all the experiments without further modifications.

These two clusters were soluble in dichloromethane (DCM), which was used as the solvent throughout the experiment, if not mentioned otherwise. About 1 mg/mL of each cluster was dissolved in DCM and mixed in a 1:1 (v/v) ratio. The mixture was stirred at room temperature for 24 h. The product formed was analyzed using UV/vis absorption spectroscopy and ESI MS.

To begin with, the inherently negatively charged Au<sub>25</sub>(PET)<sub>18</sub> showed a sharp peak at *m/z* 7393 in the negative ion ESI MS (Figure S1). On the other hand, Ir<sub>9</sub>(PET)<sub>6</sub> showed a sharp peak centered at *m/z* 2553 in the positive ion MALDI MS. When these clusters were reacted, the product had distinctly different absorption features and mass spectra. The

Received: May 1, 2017

Accepted: June 6, 2017

Published: June 6, 2017

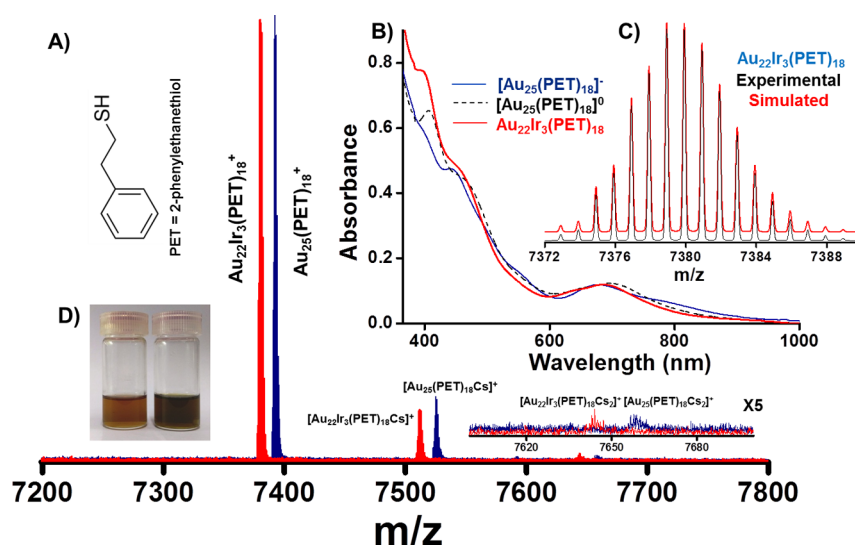


**Figure 1.** (A) ESI MS of  $\text{Au}_{22}\text{Ir}_3(\text{PET})_{18}$  (red trace) and  $\text{Au}_{25}(\text{PET})_{18}$  (blue trace) in positive ion mode. CsOAc was used as the ionization enhancer. (B) UV/vis absorption spectra of  $\text{Au}_{22}\text{Ir}_3(\text{PET})_{18}$  (red trace),  $[\text{Au}_{25}(\text{PET})_{18}]^-$  (blue trace), and  $[\text{Au}_{25}(\text{PET})_{18}]^0$  (dotted black trace) in DCM. (C) Simulated (red trace) and experimental (black trace) isotope distribution of  $\text{Au}_{22}\text{Ir}_3(\text{PET})_{18}$ . (D) Photographs of  $\text{Au}_{25}(\text{PET})_{18}$  (left) and  $\text{Au}_{22}\text{Ir}_3(\text{PET})_{18}$  (right) solutions in DCM with comparable concentrations.

product was not detected in negative ion ESI MS unlike the parent  $\text{Au}_{25}(\text{PET})_{18}$ . We presumed that this is due to the neutral charge state of the product. CsOAc was used as an ionization enhancer to detect the corresponding ion in the positive mode. Figure 1A shows the positive ion ESI MS of the reaction product (red trace) as compared to that of the  $\text{Au}_{25}(\text{PET})_{18}$ , in the neutral or oxidized form.<sup>33</sup> The neutral  $\text{Au}_{25}(\text{PET})_{18}$  was taken to ensure that both samples were measured under identical conditions. Surprisingly, a single sharp peak at  $m/z$  7380 was observed in the mass spectrum of the reaction mixture. Typically, a mixture of products is obtained during intercluster reactions.<sup>25,26</sup> Because both reactant clusters were protected with the same ligand (PET), there was no complication due to ligand exchange. The product peak was shifted by 12 mass units to the lower mass compared to  $\text{Au}_{25}(\text{PET})_{18}$ , indicating more than one Ir substitution.

The as-formed cluster was assigned as  $[\text{Au}_{22}\text{Ir}_3(\text{PET})_{18}]^+$ , based on perfect matching of the mass spectrum with the simulated spectrum (Figure 1C). Due to the presence of multiple isotopes of Ir [ $^{191}\text{Ir}$  (37.3%) and  $^{193}\text{Ir}$  (62.7%)], the distribution changed significantly from that of  $\text{Au}_{25}(\text{PET})_{18}$ . Two other smaller peaks separated by  $m/z$  133 were also seen due to Cs addition. Similar attachment was observed for the parent  $\text{Au}_{25}(\text{PET})_{18}$  cluster (blue trace) also.

In Figure 1B, the UV/vis absorption spectra of  $\text{Au}_{22}\text{Ir}_3(\text{PET})_{18}$  (red trace),  $[\text{Au}_{25}(\text{PET})_{18}]^-$  (blue trace), and  $[\text{Au}_{25}(\text{PET})_{18}]^0$  (dotted black trace) are compared. Significant variations were observed in the UV/vis absorption spectrum of  $[\text{Au}_{25}(\text{PET})_{18}]^-$  upon Ir substitution, and the spectrum resembles more closely to that of  $[\text{Au}_{25}(\text{PET})_{18}]^0$ . Observations such as the disappearance of the hump at 800 nm, appearance of a hump near 600 nm, and increased intensity of the 400 nm peak suggest that the cluster oxidizes upon Ir incorporation. We know from the literature that the peak at around 680 nm in the case of  $\text{Au}_{25}(\text{PET})_{18}$  corresponds to a LUMO  $\leftarrow$  HOMO transition, which arises entirely due to the  $\text{Au}_{13}$  core.<sup>3</sup> A slight shift of this peak in  $\text{Au}_{22}\text{Ir}_3(\text{PET})_{18}$  supports the incorporation of Ir atoms in the core of  $\text{Au}_{25}(\text{PET})_{18}$ . In Figure 1D, photographs of  $\text{Au}_{25}(\text{PET})_{18}$  (left) and  $\text{Au}_{22}\text{Ir}_3(\text{PET})_{18}$  (right)

solutions at comparable concentrations are shown. We can see from the photographs that the color changes from reddish brown to greenish brown upon Ir incorporation. We note here that the color of  $\text{Au}_{25}(\text{PET})_{18}$  changes to green upon single Pt incorporation.<sup>20</sup>

To check the effect of concentration of the reactants on the reaction, concentration-dependent experiments were conducted. Reactions were performed in three different compositions by fixing the volume of  $\text{Au}_{25}(\text{PET})_{18}$  solution (1 mg/mL) to 1 mL and varying that of the  $\text{Ir}_9(\text{PET})_6$  solution (1 mg/mL) to (i) 0.5 mL [1:0.5 (v/v) ratio], (ii) 1.0 mL [1:1 (v/v) ratio], and (iii) 1.5 mL [1:1.5 (v/v) ratio]. UV/vis absorption spectra and ESI MS of these reaction products are given in Figure S3. In the first case (1:0.5), reaction was incomplete. The UV/vis absorption spectrum and ESI MS showed the presence of unreacted  $\text{Au}_{25}(\text{PET})_{18}$  (Figure S3A,B). In the second case (1:1), the complete conversion of  $\text{Au}_{25}(\text{PET})_{18}$  to  $\text{Au}_{22}\text{Ir}_3(\text{PET})_{18}$  was observed, as discussed earlier (Figure S3C,D). In the third case (1:1.5), the absorption spectrum was featureless, indicating significant degradation of  $\text{Au}_{25}(\text{PET})_{18}$  (Figure S3E,F). The product formed was not ionizable even after adding excess CsOAc, and there was no trace of unreacted parent cluster also. Hence, we conclude that these two clusters react at an optimum composition of 1:1 (v/v) of the 1 mg/mL solution, giving complete conversion of  $\text{Au}_{25}(\text{PET})_{18}$  to  $\text{Au}_{22}\text{Ir}_3(\text{PET})_{18}$ . We assume that the Au atoms coming out of  $\text{Au}_{25}(\text{PET})_{18}$  during the formation of  $\text{Au}_{22}\text{Ir}_3(\text{PET})_{18}$  are either incorporated into  $\text{Ir}_9(\text{PET})_6$  or going into the solution as thiolates.  $\text{Ir}_9(\text{PET})_6$  does not ionize in ESI MS. Ionization occurs in MALDI, but the mass difference between Au and Ir is 5 units, which makes it difficult to detect any exchange product in MALDI MS. Due to these limitations, we were unable to detect any Au substitution into  $\text{Ir}_9(\text{PET})_6$ .

ESI MS shows (Figure 1) that  $\text{Au}_{25}(\text{PET})_{18}$  converts completely to  $\text{Au}_{22}\text{Ir}_3(\text{PET})_{18}$  upon reaction with  $\text{Ir}_9(\text{PET})_6$ , and no other products with one or two Ir incorporations were observed. From a previous report, it is known that a simple chromatographic method like thin layer chromatography (TLC) can separate clusters.<sup>34</sup> Hence, to confirm the existence

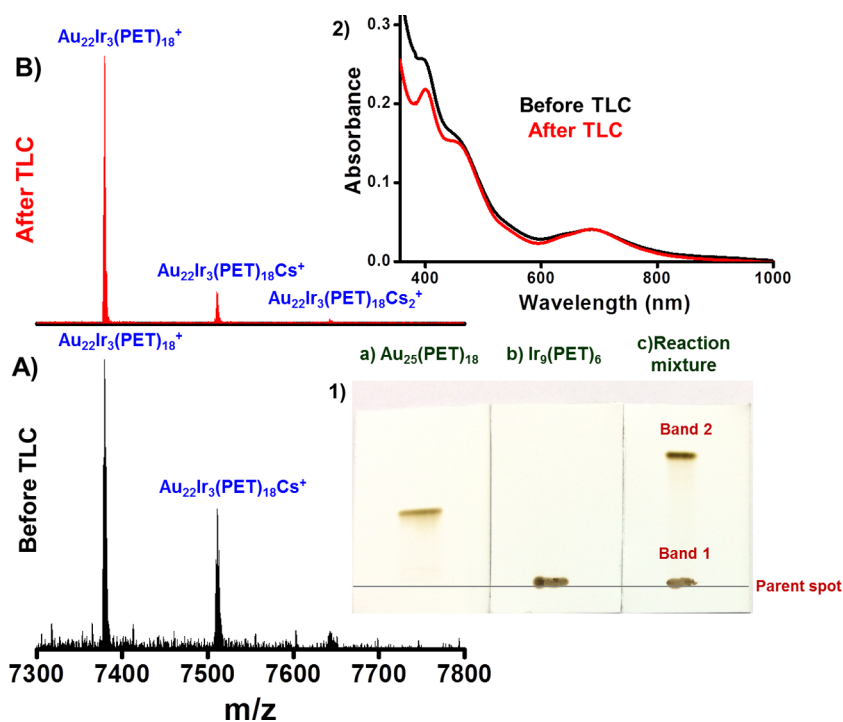


**Figure 2.** (A) ESI MS of  $\text{Au}_{22}\text{Ir}_3(\text{PET})_{18}$  before TLC compared with that after TLC. CsOAc was used as an ionization enhancer in each case. Inset (1): Photographs showing TLC plates used for the separation of (a)  $\text{Au}_{25}(\text{PET})_{18}$ , (b)  $\text{Ir}_9(\text{PET})_6$ , and (c) their reaction mixture. The mobile phase used was a 60:40 (by volume) DCM/hexane mixture. Inset (2): UV/vis absorption spectra of  $\text{Au}_{22}\text{Ir}_3(\text{PET})_{18}$  before (black trace) and after (red trace) TLC.

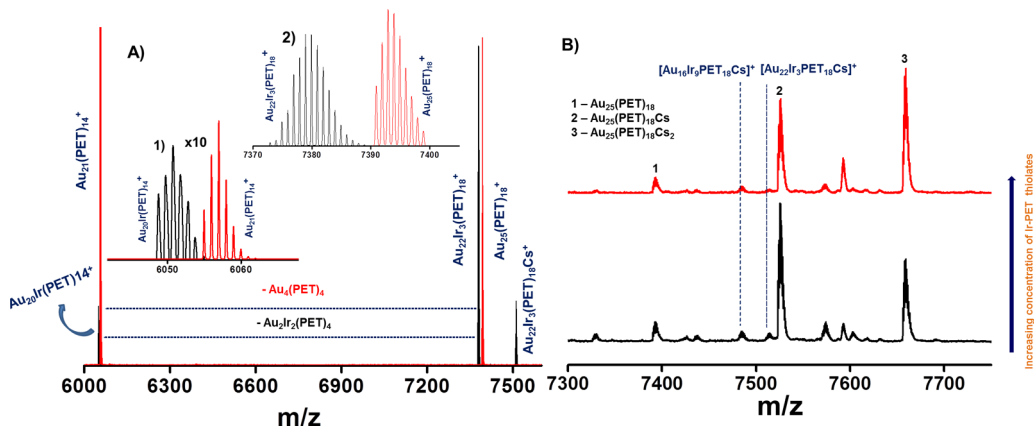


**Figure 3.** (A) ESI MS/MS of  $[\text{Au}_{22}\text{Ir}_3(\text{PET})_{18}]^+$  (black trace) compared with that of  $[\text{Au}_{25}(\text{PET})_{18}]^+$  (red trace). Inset (1) shows expansion of the fragment ion region, and (2) shows that of the parent ion peaks. (B) ESI MS of reaction between  $\text{Au}_{25}(\text{PET})_{18}$  and Ir-PET thiolates.

of a single product cluster in the reaction mixture, TLC experiments were performed. The TLC experimental conditions were adopted from the previous report,<sup>34</sup> and the same conditions were used for both the reactants and the reaction products. The mass spectrum of the cluster before TLC is shown in Figure 2A. Inset (1) of Figure 2 shows the photographs of the TLC plates used for the separation of (a)  $\text{Au}_{25}(\text{PET})_{18}$ , (b)  $\text{Ir}_9(\text{PET})_6$ , and (c) their reaction mixture.  $\text{Au}_{25}(\text{PET})_{18}$  moves on the TLC plate giving a single band, whereas  $\text{Ir}_9(\text{PET})_6$  does not move on the TLC plate at the specified conditions, forming an unmovable spot, which was nonextractable into the solvent. The reaction mixture gave two bands on the TLC plate, one unmovable (band 1) and another movable (band 2); the latter moved a different distance as compared to  $\text{Au}_{25}(\text{PET})_{18}$  under similar conditions. Band 1 was

not extractable, whereas band 2 was extracted into DCM. The solution after TLC was characterized by UV/vis absorption spectroscopy and ESI MS. The mass spectrum of the cluster after TLC is shown in Figure 2B.

This shows the peaks of  $\text{Au}_{22}\text{Ir}_3(\text{PET})_{18}$  and its Cs adducts, similar to that of the cluster before TLC. From this, it is evident that only  $\text{Au}_{22}\text{Ir}_3(\text{PET})_{18}$  was formed in the reaction. This experiment also proves that the cluster is stable and intact after TLC. Inset (2) of Figure 2 shows the UV/vis absorption spectrum of  $\text{Au}_{22}\text{Ir}_3(\text{PET})_{18}$  after TLC as compared to that of the cluster before TLC. The spectra match except for the increase in intensity of the 400 nm feature. This indicates the oxidation of the cluster upon running through the TLC plate. This was observed for  $\text{Au}_{25}(\text{PET})_{18}$  as well. The unmovable spot (band 1) in the TLC plate of the reaction mixture, which was

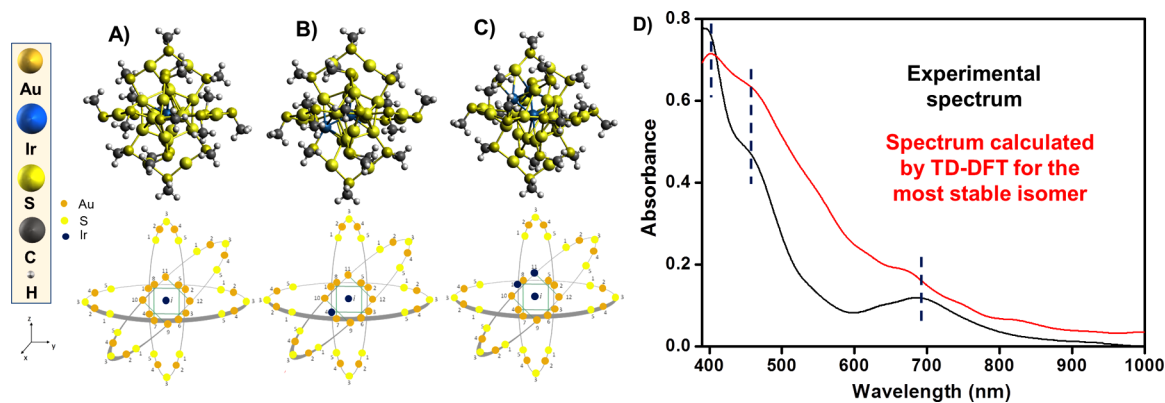


**Figure 4.** DFT-optimized structures of lowest-energy isomers of (A)  $\text{Au}_{24}\text{Ir}(\text{SMe})_{18}$ , (B)  $\text{Au}_{23}\text{Ir}_2(\text{SMe})_{18}$ , and (C)  $\text{Au}_{22}\text{Ir}_3(\text{SMe})_{18}$ . The aspicule representation of each structure is given below the structures. The positions of the Ir atoms are labeled prominently. Color code: Golden yellow, Au; bright yellow, S; blue, Ir; gray, C; and white, H. (D) Calculated UV/vis absorption spectrum for the most stable isomer of  $\text{Au}_{22}\text{Ir}_3(\text{SMe})_{18}$  (red trace) compared with the experimental spectrum (black trace).

nonextractable in any solvent, was taken to be composed of unreacted  $\text{Ir}_9(\text{PET})_6$  and other reaction products like thiolates. The TLC showed that  $\text{Au}_{22}\text{Ir}_3(\text{PET})_{18}$  is more labile than  $\text{Au}_{25}(\text{PET})_{18}$ . This indicates that the product could be neutral in comparison to the reactant, in agreement with the ESI MS study.

To get further insight into the structure of the  $\text{Au}_{22}\text{Ir}_3(\text{PET})_{18}$ , tandem mass spectrometry (ESI MS/MS) was performed.  $\text{Au}_{25}(\text{SR})_{18}$  loses  $\text{Au}_4(\text{SR})_4$  units during collision-induced dissociation (CID).<sup>35</sup> This fragmentation is one of the ways to understand whether the staple or the core of the cluster is modified by alloying. ESI MS/MS results of  $\text{Au}_{25}(\text{PET})_{18}$  and  $\text{Au}_{22}\text{Ir}_3(\text{PET})_{18}$  are compared in Figure 3A. For  $[\text{Au}_{25}(\text{PET})_{18}]^+$ , a 90 V laboratory collision energy (CE) was used to fragment the ion by CID using Ar gas.  $[\text{Au}_{21}(\text{PET})_{14}]^+$  was formed when  $\text{Au}_4(\text{PET})_4$  was lost from  $[\text{Au}_{25}(\text{PET})_{18}]^+$ . To fragment  $[\text{Au}_{22}\text{Ir}_3(\text{PET})_{18}]^+$ ,  $[\text{Au}_{22}\text{Ir}_3(\text{PET})_{18}\text{Cs}]^+$  was selected, which immediately fragmented to form  $[\text{Au}_{22}\text{Ir}_3(\text{PET})_{18}]^+$ . This was further dissociated by increasing the CE to 95 V, where a loss of  $\text{Au}_2\text{Ir}_2(\text{PET})_4$  was observed. At a similar condition,  $[\text{Au}_{22}\text{Ir}_3(\text{PET})_{18}]^+$  required more energy to fragment, indicating higher gas-phase stability of the ion compared to  $[\text{Au}_{25}(\text{PET})_{18}]^+$ .

The fragment peaks are expanded in inset (1) of Figure 3A, showing a distinctly different isotope envelope of  $[\text{Au}_{20}\text{Ir}(\text{PET})_{18}]^+$ . A comparison of isotope patterns of  $\text{Au}_{25}(\text{PET})_{18}$  and  $\text{Au}_{22}\text{Ir}_3(\text{PET})_{18}$  is presented in inset (2) of Figure 3A. The isotope pattern of the parent cluster is narrowed in the fragment ion as a consequence of the isotope distribution of the constituent elements. This further confirms the identity of the cluster.

Out of the three, two Ir atoms were lost in the fragment. This is possible if one of the Ir atoms occupies the center of the  $\text{Au}_{13}$  icosahedron. Considering the  $\text{Au}_{25}(\text{PET})_{18}$  structure, the other two Ir atoms can occupy positions either in the  $\text{Au}_2(\text{PET})_3$  staple or in the shell of the  $\text{Au}_{13}$  icosahedron. Depending on the positions of the two Ir atoms, multiple isomeric structures are possible for the cluster (discussed later).

To check the possibility of more than three Ir incorporation, multiple reactions between  $\text{Au}_{25}(\text{PET})_{18}$  and Ir-PET thiolates were conducted. Concentration-dependent reactions were performed by adding 50 and 100  $\mu\text{L}$  of Ir-PET thiolate solutions in acetonitrile to 1 mL (1 mg/mL) of the cluster

solution in DCM. The mixtures were stirred for 1 h, and the resulting products were analyzed by ESI MS (Figure 3B). Unlike the reaction with  $\text{Ir}_9(\text{PET})_6$ , this reaction was incomplete. A significant portion of  $\text{Au}_{25}(\text{PET})_{18}$  remained unreacted, as confirmed by ESI MS, where a strong signal was obtained for the parent cluster along with its Cs adducts. Multiple low-intensity peaks were observed. These peaks were assigned as  $[\text{Au}_{22}\text{Ir}_3(\text{PET})_{18}\text{Cs}]^+$  and  $[\text{Au}_{16}\text{Ir}_9(\text{PET})_{18}\text{Cs}]^+$  along with a few unassigned peaks. Different product formation in this case could be due to the difference in reactivity of Ir-PET thiolates as compared to  $\text{Ir}_9(\text{PET})_6$ . The Ir-PET thiolates could be having higher reactivity than  $\text{Ir}_9(\text{PET})_6$ , thereby leading to the formation of a product with higher Ir doping.

In these experiments, we were able to detect the  $\text{Ir}_9$  substituted product. If this kind of product was formed in reactions between  $\text{Au}_{25}(\text{PET})_{18}$  and  $\text{Ir}_9(\text{PET})_6$ , we must have been able to detect them. Hence, the monodispersity of the product formed in the former case is indirectly proven by these experiments. These also indicate higher stability of the products when Ir atoms are exchanged in multiplicities of three, compared to other possible products. It could also be possible that different metastable Ir substituted products undergo reaction among each other to form the most stable products where multiples of three Ir atoms are exchanged. However, we could not identify any such intermediate species in our time-dependent study.

To understand the substitution in detail, density functional theory (DFT) calculations were conducted. Au was replaced with Ir in  $\text{Au}_{25}(\text{PET})_{18}$  in a stepwise fashion. First, one Au was replaced with Ir, and the energy-minimized structure was calculated. Among the three possible isomers, one with Ir at the center of the  $\text{Au}_{13}$  icosahedron was most stable. This is similar to the cases of Pd in  $\text{Au}_{24}\text{Pd}(\text{SR})_{18}$ ,<sup>18</sup> Cu in  $\text{Au}_{24}\text{Cu}(\text{SR})_{18}$ ,<sup>21</sup> and Pt in  $\text{Au}_{24}\text{Pt}(\text{SR})_{18}$ ,<sup>36</sup> which preferentially occupy the center of the icosahedron. To arrive at this conclusion, an Ir atom was substituted at three different positions [center of the icosahedron, shell of the icosahedron, and staple of  $\text{Au}_{25}(\text{SR})_{18}$ ]. The optimized geometry of the most stable isomer is shown in Figure 4A, and structures of other isomers are shown in Figure S5. The aspicule representation of each structure is given below the respective DFT-optimized structure to make the representation better.<sup>37</sup> Due to the same ligand protection in the reacting clusters, the possibility of

ligand exchange was not taken into account. However, PET was replaced with  $-SMe$  to reduce the computational cost.

The calculated relative energies reveal that Ir in the center of the icosahedron is more stable than that in other positions. Substitution of Ir in the center does not disturb the symmetry of the  $Au_{25}(SMe)_{18}$  structure, whereas substitution in the staple distorts the structure significantly (Figure S5). The Ir atom on the staple is pulled towards the icosahedral core, and the angle of  $S-Ir-S$  changes to  $126^\circ$  from that of  $S-Au-S$  which is  $172.2^\circ$ . These changes cause a rise in energy compared to the substitution in the center of the icosahedron. These calculations show that the isomers with one Ir substitution, that is,  $Au_{24}Ir(SMe)_{18}$ , are stable and their formation energies are negative. Hence, the formation of one Ir substituted product in the reaction is favorable. Therefore, there is a possibility that the formation of an undetected intermediate is the driving force of the reaction. The most stable geometry with one Ir in the center of the icosahedron was used for further studies on substitution.

Two possibilities [shell of icosahedron and staple of  $Au_{25}(SMe)_{18}$ ] were considered for the substitution of the second Ir atom. The optimized geometries are displayed in Figures 4B and S5, with aspicule representations of the structures. The isomer with an Ir–Ir bond (substitution to the shell of the icosahedron) gave the lowest energy. This is likely to be due to the increased strength of Ir–Ir than Au–Au and Au–Ir bonds. The calculated bond dissociation energies follow the order Ir–Ir > Au–Au > Au–Ir, which are 385.974, 210.413, and 95.729  $\text{kJ mol}^{-1}$ , respectively. We suggest that Ir–Ir bond formation within the cluster increases its stability. Two Ir in the icosahedron, one at the center and the other on the shell, that is, structure B in Figure 4, were used for the subsequent step.

The third Ir atom was substituted in different positions of the icosahedral shell and staple of the most stable  $Au_{23}Ir_2(SMe)_{18}$  isomer. The optimized geometries with their aspicule representations are shown in Figures 4, S6, and S7. The substitution in the icosahedron leads to minimum-energy geometries when compared to the other possibilities. Three isomeric structures are possible in this case (structures A, B, and D in Figure S6), forming triangular, bent, and linear  $Ir_3$  moieties. The structure with a triangular  $Ir_3$  unit containing three Ir–Ir bonds is the lowest in energy compared to linear and bent forms (see Figures 4 and S6). The symmetrical structure of  $Au_{25}(SMe)_{18}$  undergoes less distortion in this lowest-energy geometry compared to the other structures. Several other geometries were considered from random substitution of three Ir atoms in staples and the core of  $Au_{25}(SMe)_{18}$ , which are shown in Figure S6 (structures C, E, and F) and Figure S7. The energies of these geometries are higher than the lowest-energy structure of  $Au_{22}Ir_3(SMe)_{18}$ . The results reveal that the larger number of Ir–Ir bonds and fewer distortions in geometry from the symmetrical arrangement increase the stability of the structure.

Monodispersity of the product formed in this reaction is a surprising finding as intercluster reactions generally produce a mixture of products. In the reported cases,<sup>25,26</sup> the reactions were between Au and Ag clusters, leading to the formation of Au–Ag alloy clusters. In the present case, the reaction is between Au and Ir clusters. The affinity of Au and Ag to form alloys is different from that of Au and Ir. This could be a factor determining the formation of a single product. Another aspect could be the unique structure of the  $Au_{22}Ir_3(PET)_{18}$  cluster, wherein three Ir atoms form a triangular unit within the cluster.

This could give extra stability to the cluster compared to other substitution products, forming the single alloy cluster. There must be additional factors responsible, and they need to be explored.

The theoretical UV/vis absorption spectrum for the most stable isomer of  $Au_{22}Ir_3(SMe)_{18}$  was calculated using time-dependent density functional theory (TDDFT) methods (for details, see the Supporting Information). The calculated spectrum for the most stable isomer showed good agreement with the experimental spectrum, except for the uniform red shift ( $\sim 60$  nm) of the peaks, which has been corrected and is shown in Figure 4 (the original spectrum is given in Figure S8). The reasons for this shift may be the replacement of PET ligands by SMe ligands in TDDFT calculations and errors in the TDDFT methods like the use of effective core potentials for Au and Ir atoms. These kinds of shifts are common in calculations and have been reported in the literature.<sup>3,38</sup> Important features of the cluster are marked with the dotted lines, which match with the experimental spectrum. The prominent feature at around 680 nm exhibits a shift from parent  $Au_{25}(PET)_{18}$ , as compared in Figure 1. The match between experimental and calculated spectra thus supports our structural predictions.

In conclusion, a novel alloy cluster of Ir and Au, namely,  $Au_{22}Ir_3(PET)_{18}$ , was synthesized by the reaction between  $Au_{25}(PET)_{18}$  and  $Ir_9(PET)_6$ . The formation of a single product was confirmed by TLC and ESI MS studies. Tandem mass spectrometry was used to understand the structural modification due to Ir substitution. CID of the cluster ion showed loss of  $Au_2Ir_2(PET)_4$  instead of  $Au_4(PET)_4$  [observed in the case of  $Au_{25}(PET)_{18}$ ]. To understand the structure in greater detail, DFT calculations were performed on the  $Au_{22}Ir_3(PET)_{18}$ . Substitution of one Ir atom in the center of the icosahedron and two Ir atoms in the shell of the icosahedron forming a triangular  $Ir_3$  unit leads to the lowest-energy isomer. This type of structure was not seen before for any other heteroatom substitution in  $Au_{25}(SR)_{18}$ . Study of magnetic properties due to Ir incorporation would be an immediate area of work for this newly synthesized cluster. Enhanced catalytic activity is expected due to Ir substitution, and this would be of great interest for the cluster community.

## EXPERIMENTAL METHODS

**Synthesis of  $Au_{25}(PET)_{18}$ .**  $Au_{25}(PET)_{18}$  was synthesized by the modified Brust–Schiffrin single-phase synthetic protocol.<sup>27,28</sup> Details are presented in the Supporting Information.

**Synthesis of  $Ir_9(PET)_6$ .** This cluster was synthesized following a recently reported solid-state protocol.<sup>32</sup> The procedure is described in detail in the Supporting Information.

**Reaction between  $Au_{25}(PET)_{18}$  and  $Ir_9(PET)_6$ .** Reaction between the two clusters was carried out in DCM, which is a common solvent for both of them. A 1 mg/mL solution of  $Au_{25}(PET)_{18}$  was made. To a fixed volume of this solution, different volumes of 1 mg/mL solution of  $Ir_9(PET)_6$  were added to get (v/v) ratios of 1:0.5, 1:1, and 1:1.5 of  $Au_{25}(PET)_{18}$  and  $Ir_9(PET)_6$ , respectively, in the final mixture. The reaction mixtures were stirred at room temperature for 24 h.

**Reaction between  $Au_{25}(PET)_{18}$  and Ir-PET Thiolates.** The thiolates were prepared in acetonitrile by taking a 1:4 molar ratio of  $IrCl_3 \cdot xH_2O$  and PET and stirring the mixture for about 1 h. The reaction between  $Au_{25}(PET)_{18}$  and thiolates was carried out by adding varying amounts of thiolate solution in acetonitrile (50 and 100  $\mu\text{L}$ ) to a 1 mg/mL solution of the

cluster in DCM. This reaction was faster compared to the reaction between the two clusters, and the product peaks were observed in the mass spectrum within 1 h of mixing.

## ■ COMPUTATIONAL DETAILS

The structure of Au<sub>25</sub>(SR)<sub>18</sub>, as reported previously by Heaven et al.,<sup>29</sup> was used in the present study (Figure S4). All of the calculations were performed using Gaussian 09 software.<sup>39</sup> More details are given in the Supporting Information.

## ■ ASSOCIATED CONTENT

### ■ Supporting Information

The Supporting Information is available free of charge on the ACS Publications website at DOI: 10.1021/acs.jpcl.7b01052.

Characterization of Au<sub>25</sub>(PET)<sub>18</sub> and Ir<sub>9</sub>(PET)<sub>6</sub>, effect of concentration on the reaction, structure of the Au<sub>25</sub>(SMe)<sub>18</sub>, DFT-optimized structures of different isomers of Au<sub>24</sub>Ir(SMe)<sub>18</sub>, Au<sub>23</sub>Ir<sub>2</sub>(SMe)<sub>18</sub>, and Au<sub>22</sub>Ir<sub>3</sub>(SMe)<sub>18</sub>, and energies of different structures by DFT calculations (PDF)

## ■ AUTHOR INFORMATION

### Corresponding Author

\*E-mail: pradeep@iit.ac.in.

### ORCID

V. Subramanian: 0000-0003-2463-545X

Thalappil Pradeep: 0000-0003-3174-534X

### Author Contributions

§S.B. and A.B. contributed equally

### Notes

The authors declare no competing financial interest.

## ■ ACKNOWLEDGMENTS

S.B. thanks IIT Madras for her senior research fellowship, and A.B. thanks IIT Madras for an Institute Post-Doctoral fellowship. S.K. thanks DST-INSPIRE for his senior research fellowship. We thank the Department of Science and Technology for constant support for our research program.

## ■ REFERENCES

- (1) Mathew, A.; Pradeep, T. Noble Metal Clusters: Applications in Energy, Environment, and Biology. *Part. Part. Syst. Charact.* **2014**, *31*, 1017–1053.
- (2) Jin, R.; Zeng, C.; Zhou, M.; Chen, Y. Atomically Precise Colloidal Metal Nanoclusters and Nanoparticles: Fundamentals and Opportunities. *Chem. Rev. (Washington, DC, U. S.)* **2016**, *116*, 10346–10413.
- (3) Zhu, M.; Aikens, C. M.; Hollander, F. J.; Schatz, G. C.; Jin, R. Correlating the Crystal Structure of A Thiol-Protected Au<sub>25</sub> Cluster and Optical Properties. *J. Am. Chem. Soc.* **2008**, *130*, 5883–5885.
- (4) Knoppe, S.; Hakkinen, H.; Verbiest, T. Nonlinear Optical Properties of Thiolate-Protected Gold Clusters: A Theoretical Survey of the First Hyperpolarizabilities. *J. Phys. Chem. C* **2015**, *119*, 27676–27682.
- (5) Barcaro, G.; Sementa, L.; Fortunelli, A.; Stener, M. Optical Properties of Nanoalloys. *Phys. Chem. Chem. Phys.* **2015**, *17*, 27952–27967.
- (6) Link, S.; Beeby, A.; FitzGerald, S.; El-Sayed, M. A.; Schaaff, T. G.; Whetten, R. L. Visible to Infrared Luminescence from a 28-Atom Gold Cluster. *J. Phys. Chem. B* **2002**, *106*, 3410–3415.
- (7) Zheng, J.; Nicovich, P. R.; Dickson, R. M. Highly Fluorescent Noble-metal Quantum Dots. *Annu. Rev. Phys. Chem.* **2007**, *58*, 409–431.

- (8) Chang, H.-C.; Chang, Y.-F.; Fan, N.-C.; Ho, J.-a. A Facile Preparation of High-Quantum-Yield Gold Nanoclusters: Application to Probing Mercuric Ions and Biotinols. *ACS Appl. Mater. Interfaces* **2014**, *6*, 18824–18831.

- (9) Mathew, A.; Varghese, E.; Choudhury, S.; Pal, S. K.; Pradeep, T. Efficient Red Luminescence from Organic-soluble Au<sub>25</sub> Clusters by Ligand Structure Modification. *Nanoscale* **2015**, *7*, 14305–14315.

- (10) Luo, Z.; Zheng, K.; Xie, J. Engineering Ultrasmall Water-soluble Gold and Silver Nanoclusters for Biomedical Applications. *Chem. Commun. (Cambridge, U. K.)* **2014**, *50*, 5143–5155.

- (11) Xavier, P. L.; Chaudhari, K.; Baksi, A.; Pradeep, T. Protein-protected Luminescent Noble Metal Quantum Clusters: An Emerging Trend in Atomic Cluster Nanoscience. *Nano Rev.* **2012**, *3*, 14767–14782.

- (12) Negishi, Y.; Kurashige, W.; Niihori, Y.; Nobusada, K. Toward the Creation of Stable, Functionalized Metal Clusters. *Phys. Chem. Chem. Phys.* **2013**, *15*, 18736–18751.

- (13) Kurashige, W.; Niihori, Y.; Sharma, S.; Negishi, Y. Recent Progress in the Functionalization Methods of Thiolate-Protected Gold Clusters. *J. Phys. Chem. Lett.* **2014**, *5*, 4134–4142.

- (14) Zhu, Y.; Qian, H.; Jin, R. Catalysis Opportunities of Atomically Precise Gold Nanoclusters. *J. Mater. Chem.* **2011**, *21*, 6793–6799.

- (15) Schmid, G.; Baumle, M.; Geerkens, M.; Heim, I.; Osemann, C.; Sawitowski, T. Current and Future Applications of Nanoclusters. *Chem. Soc. Rev.* **1999**, *28*, 179–185.

- (16) Daniel, M.-C.; Astruc, D. Gold Nanoparticles: Assembly, Supramolecular Chemistry, Quantum-Size-Related Properties, and Applications toward Biology, Catalysis, and Nanotechnology. *Chem. Rev. (Washington, DC, U. S.)* **2004**, *104*, 293–346.

- (17) Fields-Zinna, C. A.; Crowe, M. C.; Dass, A.; Weaver, J. E. F.; Murray, R. W. Mass Spectrometry of Small Bimetal Monolayer-Protected Clusters. *Langmuir* **2009**, *25*, 7704–7710.

- (18) Negishi, Y.; Kurashige, W.; Niihori, Y.; Iwasa, T.; Nobusada, K. Isolation, Structure, and Stability of a Dodecanethiolate-protected Pd<sub>1</sub>Au<sub>24</sub> Cluster. *Phys. Chem. Chem. Phys.* **2010**, *12*, 6219–6225.

- (19) Negishi, Y.; Iwai, T.; Ide, M. Continuous Modulation of Electronic Structure of Stable Thiolate-protected Au<sub>25</sub> Cluster by Ag Doping. *Chem. Commun. (Cambridge, U. K.)* **2010**, *46*, 4713–4715.

- (20) Qian, H.; Jiang, D.-e.; Li, G.; Gayathri, C.; Das, A.; Gil, R. R.; Jin, R. Monoplatinum Doping of Gold Nanoclusters and Catalytic Application. *J. Am. Chem. Soc.* **2012**, *134*, 16159–16162.

- (21) Negishi, Y.; Munakata, K.; Ohgake, W.; Nobusada, K. Effect of Copper Doping on Electronic Structure, Geometric Structure, and Stability of Thiolate-Protected Au<sub>25</sub> Nanoclusters. *J. Phys. Chem. Lett.* **2012**, *3*, 2209–2214.

- (22) Kurashige, W.; Munakata, K.; Nobusada, K.; Negishi, Y. Synthesis of Stable Cu<sub>n</sub>Au<sub>25-n</sub> Nanoclusters (n = 1–9) Using Selenolate Ligands. *Chem. Commun. (Cambridge, U. K.)* **2013**, *49*, 5447–5449.

- (23) Liao, L.; Zhou, S.; Dai, Y.; Liu, L.; Yao, C.; Fu, C.; Yang, J.; Wu, Z. Mono-Mercury Doping of Au<sub>25</sub> and the HOMO/LUMO Energies Evaluation Employing Differential Pulse Voltammetry. *J. Am. Chem. Soc.* **2015**, *137*, 9511–9514.

- (24) Wang, S.; Song, Y.; Jin, S.; Liu, X.; Zhang, J.; Pei, Y.; Meng, X.; Chen, M.; Li, P.; Zhu, M. Metal Exchange Method Using Au<sub>25</sub> Nanoclusters as Templates for Alloy Nanoclusters with Atomic Precision. *J. Am. Chem. Soc.* **2015**, *137*, 4018–4021.

- (25) Krishnadas, K. R.; Ghosh, A.; Baksi, A.; Chakraborty, I.; Natarajan, G.; Pradeep, T. Intercluster Reactions between Au<sub>25</sub>(SR)<sub>18</sub> and Ag<sub>44</sub>(SR)<sub>30</sub>. *J. Am. Chem. Soc.* **2016**, *138*, 140–148.

- (26) Krishnadas, K. R.; Baksi, A.; Ghosh, A.; Natarajan, G.; Pradeep, T. Structure-conserving Spontaneous Transformations between Nanoparticles. *Nat. Commun.* **2016**, *7*, 13447–13455.

- (27) Wu, Z.; Suhan, J.; Jin, R. One-pot Synthesis of Atomically Monodisperse, Thiol-functionalized Au<sub>25</sub> nanoclusters. *J. Mater. Chem.* **2009**, *19*, 622–626.

- (28) Parker, J. F.; Fields-Zinna, C. A.; Murray, R. W. The Story of a Monodisperse Gold Nanoparticle: Au<sub>25</sub>L<sub>18</sub>. *Acc. Chem. Res.* **2010**, *43*, 1289–1296.

- (29) Heaven, M. W.; Dass, A.; White, P. S.; Holt, K. M.; Murray, R. W. Crystal Structure of the Gold Nanoparticle  $[\text{N}(\text{C}_6\text{H}_{17})_4]^-[\text{Au}_{25}(\text{SCH}_2\text{CH}_2\text{Ph})_{18}]^-$ . *J. Am. Chem. Soc.* **2008**, *130*, 3754–3755.
- (30) Akola, J.; Walter, M.; Whetten, R. L.; Hakkinen, H.; Gronbeck, H. On the Structure of Thiolate-Protected  $\text{Au}_{25}$ . *J. Am. Chem. Soc.* **2008**, *130*, 3756–3757.
- (31) Negishi, Y.; Chaki, N. K.; Shichibu, Y.; Whetten, R. L.; Tsukuda, T. Origin of Magic Stability of Thiolated Gold Clusters: A Case Study on  $\text{Au}_{25}(\text{SC}_6\text{H}_{13})_{18}$ . *J. Am. Chem. Soc.* **2007**, *129*, 11322–11323.
- (32) Bhat, S.; Chakraborty, I.; Maark, T. A.; Mitra, A.; De, G.; Pradeep, T. Atomically Precise and Monolayer Protected Iridium Clusters in Solution. *RSC Adv.* **2016**, *6*, 26679–26688.
- (33) Zhu, M.; Eckenhoff, W. T.; Pintauer, T.; Jin, R. Conversion of Anionic  $[\text{Au}_{25}(\text{SCH}_2\text{CH}_2\text{Ph})_{18}]^-$  Cluster to Charge Neutral Cluster via Air Oxidation. *J. Phys. Chem. C* **2008**, *112*, 14221–14224.
- (34) Ghosh, A.; Hassinen, J.; Pulkkinen, P.; Tenhu, H.; Ras, R. H. A.; Pradeep, T. Simple and Efficient Separation of Atomically Precise Noble Metal Clusters. *Anal. Chem. (Washington, DC, U. S.)* **2014**, *86*, 12185–12190.
- (35) Fields-Zinna, C. A.; Sampson, J. S.; Crowe, M. C.; Tracy, J. B.; Parker, J. F.; de Ney, A. M.; Muddiman, D. C.; Murray, R. W. Tandem Mass Spectrometry of Thiolate-Protected Au Nanoparticles  $\text{Na}_x\text{Au}_{25}(\text{SC}_2\text{H}_4\text{Ph})_{18-y}(\text{S}(\text{C}_2\text{H}_4\text{O})_5\text{CH}_3)_y$ . *J. Am. Chem. Soc.* **2009**, *131*, 13844–13851.
- (36) Christensen, S. L.; MacDonald, M. A.; Chatt, A.; Zhang, P.; Qian, H.; Jin, R. Dopant Location, Local Structure, and Electronic Properties of  $\text{Au}_{24}\text{Pt}(\text{SR})_{18}$  Nanoclusters. *J. Phys. Chem. C* **2012**, *116*, 26932–26937.
- (37) Natarajan, G.; Mathew, A.; Negishi, Y.; Whetten, R. L.; Pradeep, T. A Unified Framework for Understanding the Structure and Modifications of Atomically Precise Monolayer Protected Gold Clusters. *J. Phys. Chem. C* **2015**, *119*, 27768–27785.
- (38) Aikens, C. M.; Schatz, G. C. Time-Dependent Density Functional Theory Examination of the Effects of Ligand Adsorption on Metal Nanoparticles. *ACS Symposium Series; Nanoparticles: Synthesis, Stabilization, Passivation, and Functionalization*; 2008; Vol. 996, pp 108–121.10.1021/bk-2008-0996.ch009
- (39) Frisch, M. J.; Trucks, G. W.; Schlegel, H. B.; Scuseria, G. E.; Robb, M. A.; Cheeseman, J. R.; et al. *Gaussian 09*, revision A 02; Gaussian, Inc.: Wallingford, CT, 2009.